Numerical Simulation of Hydrodynamics and Cracking Reactions in the Feed Mixing Zone of a Multiregime Gas−Solid Riser Reactor

ARTICLE *in* INDUSTRIAL & ENGINEERING CHEMISTRY RESEARCH · OCTOBER 2011

Impact Factor: 2.59 · DOI: 10.1021/ie100232h

5 AUTHORS, INCLUDING:

Gan Jieqing
Monash University (Australia)
8 PUBLICATIONS **36** CITATIONS
SEE PROFILE

Hui Zhao
China University of Petroleum
11 PUBLICATIONS **55** CITATIONS
SEE PROFILE

Abdallah S Berrouk
Petroleum Institute (UAE)
59 PUBLICATIONS **221** CITATIONS
SEE PROFILE

I&EC research
Industrial & Engineering Chemistry Research

ARTICLE

pubs.acs.org/IECR

Numerical Simulation of Hydrodynamics and Cracking Reactions in the Feed Mixing Zone of a Multiregime Gas−Solid Riser Reactor

Jieqing Gan,[†] Hui Zhao,[*,†] Abdallah S. Berrouk,[*,‡] Chaohe Yang,[†] and Honghong Shan[†]

[†]State Key Laboratory of Heavy Oil Processing, China University of Petroleum, Qingdao 266555, China

[‡]Chemical Engineering Department, Petroleum Institute, Abu Dhabi 2533, United Arab Emirates

ABSTRACT: A CFD simulation was performed to evaluate the performance of a novel multiregime gas−solid fluidized riser reactor that was designed to maximize the propylene yield from the catalytic cracking process. Simulation results of the industrial-scale riser reactor show the coexistence of different regimes in the reactor. Also, both the outlet product compositions and the reaction rate vectors indicate that the cracking reactions mainly take place in the feed injection section. The product quality and distribution demonstrate the superiority of this novel process technology. The results of the CFD simulations are in good agreement with the test run results of a real industrial FCC reactor.

1. INTRODUCTION

The global demand for propylene is growing faster than the anticipated supply from ethylene plants. Fluid catalytic cracking (FCC) units, as the second largest source of propylene (about 30%), are expected to bridge much of the propylene supply/demand gap. Consequently, many special specific propylene processes have emerged to respond to the market's evolving needs for propylene. Among these propylene-producing processes include are the atmospheric residue maximizing gas and gasoline (ARGG) process,[1] deep catalytic cracking (DCC),[2,3] the maximizing isoparaffins with cleaner gasoline and propylene (MIP-CGP) process,[4] PetroFCC,[5] and two-stage-riser catalytic pyrolysis for maximizing propylene yield (TMP).[6] The success of these technologies confirms that heavy-oil catalytic cracking/pyrolysis is a promising process for converting low-value heavy oil into more valuable light olefins such as ethylene and propylene.

Until now, most of the research on FCC riser reactors has focused on either reactor hydrodynamics or catalytic cracking/pyrolysis kinetics. Both aspects are of crucial importance for reactor simulation and design, catalytic reaction control, and operating condition optimization. The flow behavior in the riser can be investigated by cold model experiments.[7−9] However, many of these studies have been confined to the macroscopic observations because of severe limits imposed by the measuring instruments and conditions. In actual industrial-scale experiments, primary attention has been paid to the final product components and product quality, whereas concern is rarely focused on the local reaction pattern. In the past decade, with the development of computer hardware and computational techniques, computational fluid dynamics (CFD) has become a powerful tool for studying flow and reaction behavior within chemical reactors, and it is becoming widely applied to investigate the effects of the design and operating conditions of FCC riser reactors on their performance.[10−12]

Heavy-oil catalytic cracking/pyrolysis involves a complicated reaction system. The first step to investigate the reaction behavior in a riser is to develop suitable kinetic models. Recently, many lumping models for catalytic cracking have been developed,[13−16] whereas reports are few regarding lumping kinetic models for catalytic pyrolysis. Among these models are the four-lump model of Xu[17] developed for DCC technology, a five-lump model proposed by Meng et al.[18] for heavy-oil contact cracking (HCC) technology, a 16-lump model established by Wang et al.,[19] and a seven-lump model developed by Li et al.[20] for the catalytic pyrolysis process (CPP). For TMP technology, a seven-lump model[21] and a further-elaborated 11-lump model[22] were developed by our research group to meet the increasing demand for this process technology led by the fast-growing propylene market.

The riser reactor is the core of any FCC unit. It can be divided into four parts based on the role played in the catalytic cracking/pyrolysis process: the prelift zone, the feedstock injection zone, the full reaction zone, and the quenching zone. It is well-known that the feedstock injection zone is the most important, yet complex, part of the riser reactor. Indeed, this is where high-velocity injection of feed oil and atomizing steam and acceleration of catalysts take place, and more importantly, this is where catalytic cracking reactions occur. Research on the feedstock injection zone of the riser reactor published in the open literature has focused mainly on the flow behavior in this zone and has been scarce until recently.[23,24]

In the present study, a three-dimensional two-phase flow-reaction simulation was carried out based on the two-fluid model (TFM) and an 11-lump kinetic model of TMP. Local hydrodynamics and cracking reaction behaviors in the feed mixing section of the TMP riser were studied in detail. The predicted results were then compared with the operating data of a commercial riser reactor.

Received: February 1, 2010
Accepted: August 29, 2011
Revised: August 28, 2011
Published: August 29, 2011

dx.doi.org/10.1021/ie100232h | *Ind. Eng. Chem. Res.* 2011, 50, 11511–11520

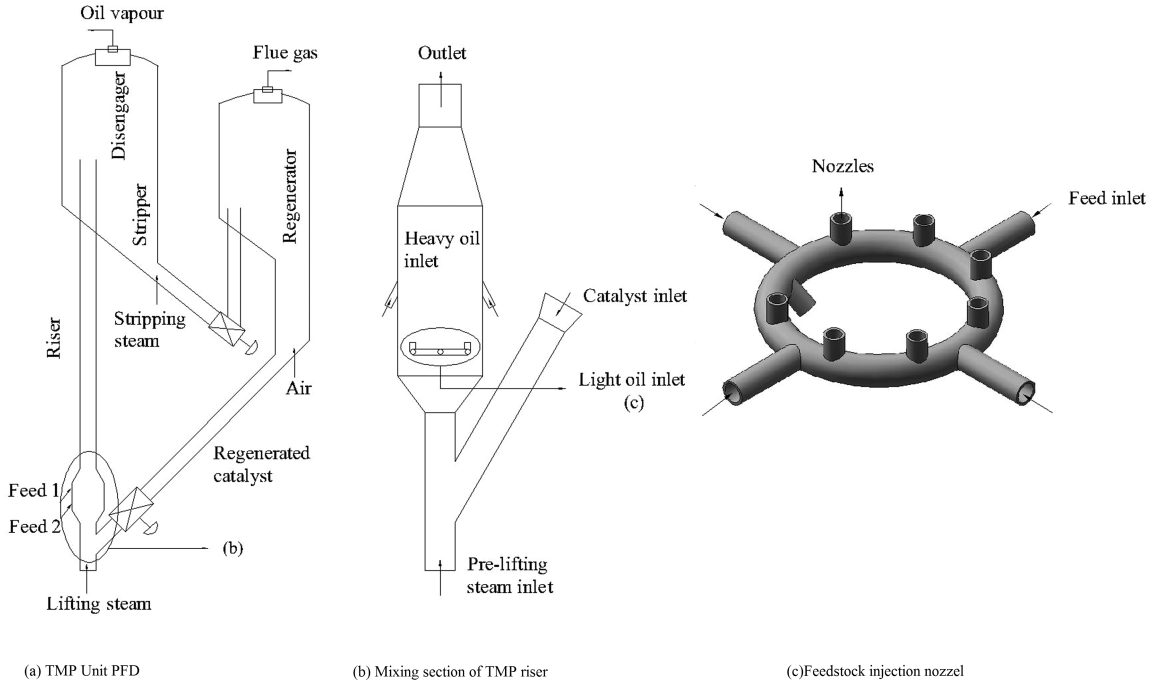

Figure 1. Schematic of the TMP riser reactor unit with stratified injections.

2. PROCESS DESCRIPTION

Figure 1a shows a typical TMP setup, which consists of two riser reactors and a regenerator. The cracking reaction of the hydrocarbon feedstock takes place in the riser, whereas the regenerator reactivates the catalysts by burning the coke deposited on them. The TMP process is based on the two-stage reactor FCC (TSRFCC) technology.[25] The first stage of the riser deals with atmospheric residue and C_4 mixture gas, whereas the second stage is fed with recycle oil and light gasoline, both coming from the first stage. The feed is injected at the bottom of each stage along with a small amount of steam to prompt atomization and reduce coke formation. The feed is subsequently vaporized when it comes into contact with hot catalyst particles flowing from the regenerator. The hydrocarbon vapors go through endothermic catalytic cracking reactions on their way through the riser. Lighter hydrocarbons are produced as the main cracking products, along with a coke byproduct that deposits on the catalyst surface, hence reducing its activity.

The detailed structure of the combined feeding system is shown in Figure 1b. Laboratory-scale experimental studies have indicated that C_4 mixture gas or light gasoline is an ideal component to promote propylene yield.[26] The preferred reaction conditions for C_4 mixture gas or light gasoline is high reaction temperature, high catalyst-to-oil ratio, and suitable residence time. However, for heavy oil, reaction temperature should be kept at low values to avoid excess reaction. To ensure suitable reaction conditions for both heavy oil and C_4 mixtures (sometimes for light gasoline as well), a fuel-stratified injection technique was implemented. First, the low-temperature C_4/light gasoline contacts the high-temperature catalysts to produce a large amount of $C_3^=$ and decrease the catalyst temperature. The latter is due to the endothermicity of the cracking reaction and the heat transfer between the gas and solid phases. Subsequently, the low-temperature catalysts (compared to the fresh catalysts) contact heavy oil (AR or recycle oil), giving rise to low-temperature cracking reactions. The latter can stop the cracking reactions of light olefins, as the absorption ability of heavy oil is stronger than that of light oil. This ensures a short reaction time for the light oil. Moreover, low-temperature reactions can also reduce the unwanted secondary reactions and minimize high-temperature thermal cracking. To obtain a better distribution of light oil, an annular pipe with multiple nozzles was employed in this work (Figure 1c).

The geometry of the riser reactor has a significant impact on the gas−solid two-phase flow behavior. For the traditional riser (constant-diameter riser), typical core−annulus structures and serious back-mixing behavior were observed. This disfavors the much-needed contact between reactants and catalysts and could have adverse effects on the yields of the desired products. Therefore, an appropriate change to the riser geometry should be sought to improve the contact efficiency between reactants and catalysts. Our preliminary experimental study[27] showed that a changing-diameter riser could enhance contact efficiency between reactants and catalysts in the bottom part of the riser. Thus, a changing-diameter riser was used in conjunction with the TMP process. The ratio of the expanding section, D, to the original diameter, d, is taken equal to 2.0.

3. MATHEMATICAL MODEL

In this work, only the second stage of the TMP riser was simulated because of a lack of suitable reaction kinetic models for both atmospheric residue and C_4 mixture gas. A three-dimensional Euler−Euler CFD model was employed. It was coupled to a three-dimension two-phase flow-reaction to simulate the heavy-oil catalytic pyrolysis in the second stage of TMP riser reactor. The reaction behavior was described using the 11-lump kinetic model.[22] Also, it was assumed that all of the feed oil was completely vaporized at the feed inlet. Indeed, Buchanan[28] found that for typical FCC conditions, the time required for complete vaporization of a 100-μm droplet ranges from 0.3 to 30 ms, which

Table 1. List of Constitutive Equations of the Kinetic Theory of Granular Flow (KTGF)

parameter	KTGF correlations used in the CFD model
granular viscosity	$\mu_s = \mu_{s,col} + \mu_{s,kin} + \mu_{s,fr}$
collision viscosity	$\mu_{s,col} = \frac{4}{5}\varepsilon_s\rho_s d_s g_0 \pi(1+e)\left(\frac{\Theta_s}{\pi}\right)^{1/2}$
kinetic viscosity	$\mu_{s,kin} = \mu_{s,kin,gran} + \mu_{s,kin,bulk}$
	$\mu_{s,kin,gran} = \frac{10\rho_s d_s\sqrt{\Theta_s\pi}}{96(1+e)g_0}\left[1+\frac{4}{5}g_0\varepsilon_s(1+e)\right]^2$
	$\mu_{s,bulk} = \frac{4}{3}\varepsilon_s\rho_s g_0(1+e)\sqrt{\frac{\Theta_s}{\pi}}$
frictional viscosity	$\mu_{s,fr} = 0$
energy-transfer coefficient	$k = \frac{2k_{dil}}{(1+e)g_0}\left[1+\frac{6}{5}g_0\varepsilon_s(1+e)\right]^2 + 2{\varepsilon_s}^2\rho_s d_s(1+e)g_0\left(\frac{\Theta}{\pi}\right)^2$
	where
	$k_{dil} = \frac{75\sqrt{\pi}}{384}\rho_s d_s {\Theta_s}^{1/2}$
N. Yang drag model[36]	$\beta = \begin{cases} \frac{3}{4}C_D\frac{\varepsilon_g\varepsilon_s\rho_g\lvert V_g - V_s\rvert}{d_s}\omega & \varepsilon_g \geq 0.74 \\ 150\frac{\varepsilon_s^2\mu_g}{\varepsilon_g d_s^2} + 1.75\frac{\varepsilon_s\rho_g\lvert V_g - V_s\rvert}{d_s} & \varepsilon_g < 0.74 \end{cases}$
	where
	$\omega = \begin{cases} -0.576 + \frac{0.0214}{4(\varepsilon_g - 0.7463)^2 + 0.0044} & 0.74 \leq \varepsilon_g \leq 0.82 \\ -0.0101 + \frac{0.0038}{4(\varepsilon_g - 0.7789)^2 + 0.0040} & 0.82 \leq \varepsilon_g \leq 0.97 \\ -31.8295 + 32.8295\varepsilon_g & \varepsilon_g > 0.97 \end{cases}$
	$C_D = \begin{cases} \frac{24}{Re}[1 + 0.15(Re)^{0.687}] & Re < 1000 \\ 0.44 & Re \geq 1000 \end{cases}$
	$Re = \frac{\varepsilon_g\rho_g d_s\lvert V_g - V_s\rvert}{\mu_g}$

is much shorter than the residence time of feed oil in the present numerical simulations.

3.1. Conservation Equation. An Euler−Euler model, closed using the kinetic theory of granular flow, was used to model the hydrodynamics of the gas−solid flow in the riser section of the FCC reactor. One set of mass and momentum conservation equations was solved for each phase. Momentum equations for both phases were linked by an interphase exchange term. The model governing equations for the gas and solid phases are as follows:

Continuity equation for the gas phase

$$\frac{\partial}{\partial t}(\varepsilon_g\rho_g) + \nabla\cdot(\varepsilon_g\rho_g V_g) = 0 \quad (1)$$

Continuity equation for the particulate phase

$$\frac{\partial}{\partial t}(\varepsilon_s\rho_s) + \nabla\cdot(\varepsilon_s\rho_s V_s) = 0 \quad (2)$$

Momentum equation for the gas phase

$$\frac{\partial}{\partial t}(\varepsilon_g\rho_g V_g) + \nabla\cdot(\varepsilon_g\rho_g V_g V_g) = -\varepsilon_g\nabla P + \varepsilon_g\rho_g g + \nabla\cdot\tau_g - \beta_{gs}(V_g - V_s) \quad (3)$$

Momentum equation for the particulate phase

$$\frac{\partial}{\partial t}(\varepsilon_s\rho_s V_s) + \nabla\cdot(\varepsilon_s\rho_s a V_s V_s) = -\varepsilon_s\nabla P + \varepsilon_s\rho_s g + \nabla\cdot\tau_s - \beta_{gs}(V_s - V_g) \quad (4)$$

Continuity between the two phases

$$\varepsilon_g + \varepsilon_s = 1 \quad (5)$$

The component continuity equation of the gas phase taking into account cracking reactions taking place in the gas phase

reads

$$\frac{\partial}{\partial t}(\varepsilon_g \rho_g Y_j) + \nabla\cdot(\varepsilon_g \rho_g V_g Y_j) = \nabla\cdot(\varepsilon_g \rho_g D \mathrm{grad}(Y_S)) + W_j \quad (6)$$

where W_j is the reaction rate ($kg\cdot m^{-3}\cdot s^{-1}$).

The energy equation for the gas phase accounting for the heat transfer between the hot particulate phase and the gas phase and the endothermicity of the reactions in the gas phase reads

$$\frac{\partial}{\partial t}(\varepsilon_g \rho_g C_p T) + \nabla\cdot(\varepsilon_g \rho_g V_g C_p T) = \nabla\cdot[\lambda\cdot\mathrm{grad}(T)] - \sum_{j=1}^{n} W_j Q_{rj} + Q_{sg} \quad (7)$$

The energy equation for the particulate phase reads

$$\frac{\partial}{\partial t}(\varepsilon_s \rho_s C_{ps} T_s) + \nabla\cdot(\varepsilon_s \rho_s V_s C_p T_s) = -Q_{sg} \quad (8)$$

where Q_{sg} is the interphase heat-transfer term ($kg\cdot m^{-3}\cdot s^{-1}$) and Q_{rj} is the reaction heat ($kg\cdot m^{-3}\cdot s^{-1}$). The latter is calculated based on the molecular expansion method.[29]

3.2. Constitutive Equations. To close the governing equations, the particulate-phase properties should be defined, and appropriate closure laws for both phases stress tensors, particulate-phase pressure, and momentum interphase coefficient must be established.

In this work, the particulate-phase properties were derived based on the kinetic theory of granular flow (KTGF).[30] The conservation equation for the fluctuation energy of the particulate phase, known as the granular temperature, Θ_s, can be obtained by solving its transport equation, which reads

$$\frac{3}{2}\left[\frac{\partial}{\partial t}(\rho_s \varepsilon_s \Theta_s) + \nabla\cdot(\rho_s \varepsilon_s V_s \Theta_s)\right] = (-P_s I + \tau_s)\cdot\nabla V_s - \nabla\cdot(k_{\Theta_s}\nabla\Theta_s) - \gamma_s\Theta_s + \phi_{gs} \quad (9)$$

where k_{Θ_s} is the thermal diffusion coefficient, $\gamma_s\Theta_s$ is the collision dissipation energy, and ϕ_{gs} is the transfer of kinetic energy between gas and particulate phases. Definitions for these terms are given in Table 1.

The stress tensors for the two phases can be expressed as

$$\tau_g = \varepsilon_g \mu_g \left\{[\nabla u_g + (\nabla u_g)^T] - \frac{2}{3}(\nabla u_g) I\right\} \quad (10)$$

$$\tau_s = [-\varepsilon_g p_s + \varepsilon_g \lambda_s (\nabla u_s)] I + \varepsilon_s \mu_s \left\{[\nabla u_s + (\nabla u_s)^T] - \frac{2}{3}(\nabla u_s) I\right\} \quad (11)$$

The particulate-phase pressure, P_s, is derived based on the kinetic theory of granular flow and reads

$$P_s = \varepsilon_s \rho_s \Theta_s [1 + 2 g_0 \varepsilon_s (1 + e)] \quad (12)$$

The radial distribution function, g_0, is interpreted as the probability of a single particle colliding with another particle in the particulate phase. Thus, its value increases with increasing solid volume fraction. In this study, the following expression was used

$$g_0 = \frac{1}{1 - (\varepsilon_s/\varepsilon_{s,\max})^{1/3}} \quad (13)$$

The drag force between the gas and particulate phases is one of the dominant forces in a fluidized bed. Drag laws, which are applied to model the momentum exchange between phases, are often developed empirically. Several drag models available in the literature are applicable to gas−solid flows in riser reactors. We mention, herein, those of Wen and Yu,[31] Di Felice,[32] Ergun,[33] Gidaspow et al.,[34] Syamlal and O'Brien,[35] and Yang et al.[36] The Yang et al. model is derived based on the energy-minimization multiscale (EMMS)[37] approach and it takes the particle acceleration into consideration. Its parameters are detailed in Table 1. This drag model was used in the present work.

3.3. Reaction Kinetics. According to the 11-lump[22] kinetic model, the pyrolysis gas was divided into heavy oil (HO), diesel oil (DO), gasoline [olefin (G^O), aromatic (G^A), saturates (G^S)], LPG [butane + propane ($C_{3,4}{}^0$), butylene ($C_4{}^=$), propylene ($C_3{}^=$)], dry gas [ethane ($DG^=$), ethane + methane + H_2 (DG^0)], and coke (CK) (see Table 2). The reaction schemes are shown in Figure 2, and the corresponding kinetic parameters are listed in Table 3. Therein, reaction heat is calculated based on the molecular expansion method.[29]

Table 2. Lumping of TMP Reaction System

lump symbol	lump name	boling range
HO	heavy oil	350−500 °C
DO	diesel oil	204−350 °C
G^O	gasoline olefin	C_5−204 °C
G^A	gasoline aromatic	C_5−204 °C
G^S	gasoline saturated hydrocarbon	C_5−204 °C
$C_{3,4}{}^0$	butane + propane	$C_4{}^0 + C_3{}^0$
$C_4{}^=$	butylene	$C_4{}^=$
$C_3{}^=$	propylene	$C_3{}^=$
$DG^=$	ethene	$C_2{}^=$
DG^0	ethane + methane + H_2	$C_2{}^0 + C_1 + H_2$
CK	coke	−

The deactivation function a of the catalyst particles is expressed as[22]

$$a = \frac{1}{1 + \frac{3.68N}{100R_{CO}}} \frac{1}{1 + \frac{2.10A_h}{100R_{CO}}} (1 + 14.36C_c)^{-0.20} \quad (14)$$

where the values of deactivation constants N and A_h are 0.1 and 22.64, respectively (data from Daqing AR),[22] and C_c is the coke concentration on the catalysts ($C_c = y_k/R_{CO}$, where y_k represents the mass fraction of coke in the 11 lumps).

The reaction rate constants for propylene formation at 853 K are listed in Table 4 following the 11-lump kinetic model. In addition to heavy oil and diesel oil, gasoline, especially its olefin components, has a high capacity for improving the propylene yield. However, the olefin in gasoline is unfavorable for improving the gasoline quality. Therefore, the use of a stratified feed of gasoline and heavy oil was proposed to realize complementary strengths and weaknesses. In addition, Li[26] showed that light gasoline [final boiling point (FBP) is about 340 K] that is rich in $C_5{}^=\sim C_6{}^=$ has a higher propylene yield than heavy oil and full-cut gasoline. As a result, only the light gasoline was recycled to

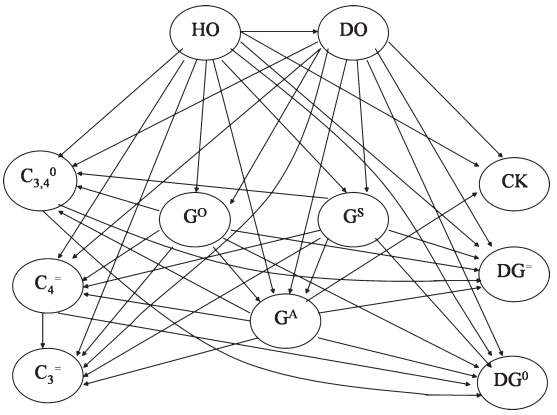

Figure 2. Reaction network of the 11-lump kinetic model.

improve the-propylene yield and simultaneously maintain the content of part of the low-carbon olefins. This contributes also in reducing the loss of gasoline.

4. COMPUTATIONAL DOMAIN AND BOUNDARY CONDITIONS

4.1. Computational Domain. Based on the experimental measuremenst[26] carried out on a laboratory-scale apparatus, a detailed design for a 120 kton/year industrial FCC unit with the same reactor geometry was proposed.

Because the feed stock injection zone is the most complicated and important part of the riser reactor, the main focus of this work is on the feed injection zone of the industrial riser reactor, even though the entire riser was simulated. The geometry of the feed injection zone used in this work is shown in Figure 1b. Prelifting steam enters from the bottom part of the riser, light gasoline enters from the middle nozzles, and the heavy oil is injected from the upper nozzles. The total mesh number of the entire riser was about 140000, and that of the feed injection zone was around 100000.

To compare the performance of the changing-diameter riser with that of the traditional straight tube riser, simulation of the feed injection zone of the traditional riser with the same feed rate and feed height was also performed. The total mesh number of the traditional riser was about 80000.

4.2. Boundary and Initial Conditions. The properties of the feed oil and solid catalysts of the TMP reactor are listed in Table 5. They were obtained through industrial data calibration. The simulation conditions of the second stage of the TMP riser reactor are summarized in Table 6. The inlet velocity was set for both the gas phase and the particle phase. The inlet velocity of the catalyst particles was calculated based on the catalyst mass flux and its inlet volume fraction

$$u_s = \frac{G_{s,in}A_{in}}{\rho_s \varepsilon_s A_s} \quad (15)$$

The inlet volume fraction of the catalyst particles was set to 0.6. The outlet of the reactor was set to atmospheric pressure. No-slip boundary conditions were set for the gas phase at the wall, and Johnson and Jackson's[38] partial-slip boundary conditions were employed for the particulate phase.

4.3. Simulation Time Parameters. To avoid numerical instabilities and convergence problems that often accompany multiphase flow simulations, a very small time step (1×10^{-4} s) with around 20 iterations per time step was chosen to reach convergence. A convergence criterion of 10^{-3} for each scaled residual component was specified for the relative error between two successive iterations. A total simulation time much greater than the mean gas residence time (25 s) was selected to ensure that the simulation duration was long enough to establish the desired operating conditions. Because of the large number of meshes and components involved in the calculations, parallel computations were performed on a single machine. The whole computation process took about 3 months. Time-averaged distributions of variables were computed covering a period of the last 10 s of the simulation time.

Table 3. Kinetic Parameters of the 11-Lump Kinetic Model

path number	reaction path	k_0 (s^{-1})	E_a ($kJ \cdot mol^{-1}$)	ΔH_r ($kJ \cdot kg^{-1}$)
1	HO → DO	601.20	59.14	180.27
2	HO → G^O	1.16×10^4	79.48	914.80
3	HO → G^A	1.58×10^6	117.17	795.52
4	HO → G^S	470.83	63.74	720.97
5	HO → $C_{3,4}^{0}$	0.43	23.67	1348.07
6	HO → $C_4^=$	14.69	35.32	1205.55
7	HO → $C_3^=$	8.29	30.44	1690.13
8	HO → $DG^=$	6.59	38.79	2659.30
9	HO → DG^0	2.12×10^5	114.75	3822.30
10	HO → CK	28.49	47.10	0.00
11	DO → G^O	2.68×10^3	75.32	734.53
12	DO → G^A	2.04×10^5	108.27	615.24
13	DO → G^S	252.49	63.15	540.69
14	DO → $C_{3,4}^{0}$	2.98	31.61	1167.80
15	DO → $C_4^=$	324.39	61.95	1025.28
16	DO → $C_3^=$	542.64	65.35	1509.86
17	DO → $DG^=$	1.27×10^4	97.64	2479.03
18	DO → DG^0	2.05×10^3	80.66	3642.03
19	DO → CK	271.60	64.40	−180.27
20	G^O → G^A	128.29	76.48	−51.28
21	G^O → $C_{3,4}^{0}$	4.28	55.17	186.27
22	G^O → $C_4^=$	61.12	58.69	125.00
23	G^O → $C_3^=$	574.14	74.72	333.33
24	G^O → $DG^=$	89.57	68.12	750.00
25	G^O → DG^0	0.45	47.86	1250.00
26	G^A → $C_{3,4}^{0}$	5.46	53.23	237.56
27	G^A → $C_4^=$	48.64	59.38	176.28
28	G^A → $C_3^=$	33.10	57.62	384.62
29	G^A → $DG^=$	6.12	48.32	801.28
30	G^A → DG^0	73.92	73.96	1301.28
31	G^A → CK	0.61	24.26	−342.01
32	G^S → G^A	0.96	32.68	32.05
33	G^S → $C_{3,4}^{0}$	0.69	32.60	269.61
34	G^S → $C_4^=$	167.09	66.27	208.33
35	G^S → $C_3^=$	105.06	63.51	416.67
36	G^S → $DG^=$	324.79	73.04	833.33
37	G^S → DG^0	2.13×10^3	94.81	1333.33
38	$C_{3,4}^{0}$ → $DG^=$	2.03×10^5	117.70	563.73
39	$C_{3,4}^{0}$ → DG^0	565.03	74.11	1063.73
40	$C_4^=$ → $C_3^=$	1.18×10^3	90.51	208.33
41	$C_4^=$ → DG^0	351.03	80.14	1125.00

Table 4. Reaction Rate Constants for Propylene Formation at 853 K

reaction route	reaction rate constant
heavy oil → propylene	0.1134
diesel oil → propylene	0.0541
gasoline olefin → propylene	0.0153
gasoline aromatic → propylene	0.0098
gasoline saturates → propylene	0.0136
butylenes → propylene	0.0034

Table 5. Feed Oil and Solid Catalyst Properties of the TMP Reactor

parameter	value
Heavy Oil	
density (293.15 K), ($kg \cdot m^{-3}$)	1070
SARA (wt %)	
saturates	33.46
aromatics	52.26
resins	13.43
asphaltenes	0.85
M (g/mol)	328
Light Gasoline	
density (293.15 K), ($kg \cdot m^{-3}$)	672.0
saturates (wt %)	30.43
aromatics (wt %)	1.31
olefins (wt %)	68.26
M (g/mol)	76.5
Solid Catalysts	
particle density ($kg \cdot m^{-3}$)	1700
d_p (μm)	76

Table 6. Simulation Conditions of the Second Stage of the TMP Riser Reactor

parameter	value
prelift steam feed rate ($kg \cdot h^{-1}$)	114
blow and start steam feed rate ($kg \cdot h^{-1}$)	144
atomizing steam feed rate ($kg \cdot h^{-1}$)	201
recycled oil feed rate ($kg \cdot h^{-1}$)	3330
light gasoline feed rate ($kg \cdot h^{-1}$)	4775
prelift steam inlet temperature (K)	500
recycled oil inlet temperature (K)	528
light gasoline inlet temperature (K)	323
catalyst inlet temperature (K)	960
prelift steam inlet velocity ($m \cdot s^{-1}$)	1.69
recycled oil inlet velocity ($m \cdot s^{-1}$)	70
light gasoline inlet velocity ($m \cdot s^{-1}$)	73.66
catalyst inlet volume fraction	0.6

5. COMPUTATIONAL RESULTS AND DISCUSSION

Figure 3 shows the time-averaged axial solid volume fractions for both the traditional riser and the changing-diameter riser. The solid holdup at the bottom part (feed inlet zone) of the changing-diameter riser is much higher than that of the traditional riser. At the upper part of this zone, the solid volume fractions of the two geometries are very similar. The facet-averaged catalyst axial velocities at different heights above the heavy-oil nozzles are shown in Table 7. The catalyst velocity in the lower part for changing-diameter riser is much lower than that in the traditional riser as a result of the enlargement of the riser diameter. At the upper part of the feed injection zone, which is the dilute-phase conveying zone, the catalyst velocity of the changing-diameter riser is close to that of the traditional riser. These results indicate that the catalyst residence time for the changing-diameter riser is relatively longer than that of the traditional riser, which contributes to a better contact between oil and catalyst particles.

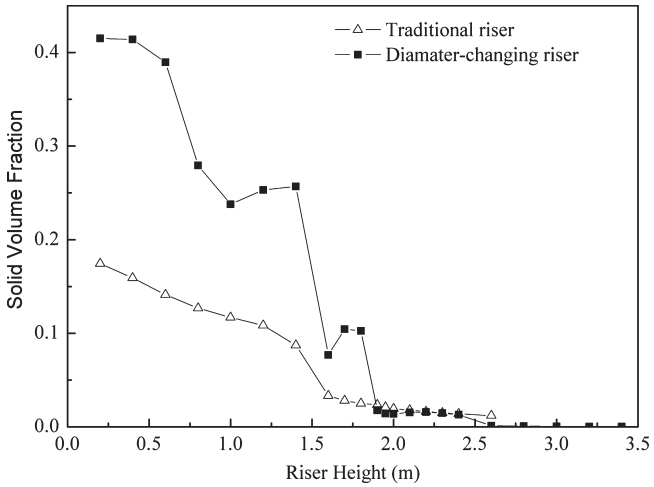

Figure 3. Predicted axial solid volume fraction for two different riser geometries.

Table 7. Facet-Averaged Catalyst Axial Velocities at Different Heights ($m \cdot s^{-1}$)

height (m)	traditional riser	changing-diameter riser
1.8	2.02	0.08
1.9	2.47	0.32
2.0	4.30	0.25
2.2	5.01	1.63
2.5	7.60	1.94
2.9	8.73	2.15
3.0	9.13	8.03

Figure 4 displays the solid-phase distribution and flow field in the lower part of the TMP riser reactor. A dense catalyst bed, which is suitable for gasoline olefin reactions, can be maintained at proper locations in the riser reactor by fine-tuning the nozzle configuration and the reactor geometry. In the lower part of the mixing zone, the superficial gas velocity is less than 3 $m \cdot s^{-1}$, and it increases to 10−15 $m \cdot s^{-1}$ in the upper part. This high-velocity span in this zone leads to the coexistence of both dense and dilute phases. These results further indicate that the TMP changing-diameter riser exhibits distinct advantages over the traditional configuration in improving the gas−solid contact efficiency at the bottom part of riser. This favors the conversion of light gasoline to light olefins. It is worth noticing that the cross-sectional solid concentration profile is not symmetrical because

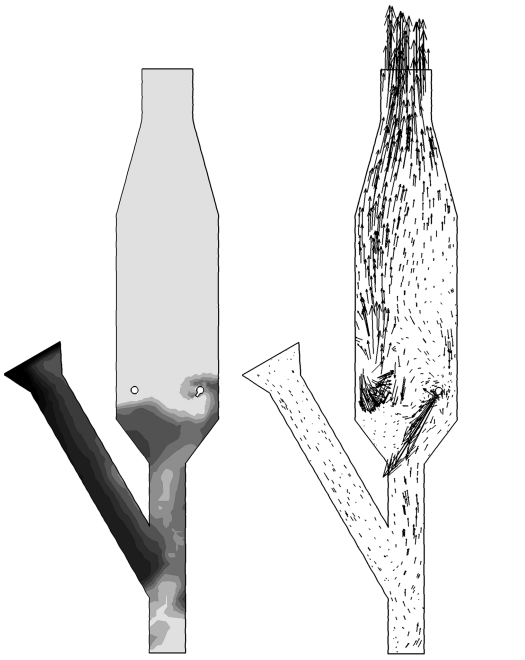

Figure 4. Phase distribution and flow field in the lower part of the riser reactor.

of the downward oblique nozzle used in the light gasoline injection system. Indeed, the dense bed height on the oblique downward nozzle side is higher than that on the other side of the system; hence, the catalyst phase takes on bias flow behavior.

A comparison of the numerical predictions of the outlet compositions of the feed mixing section to the industrial experimental results for the whole riser is presented in Table 8. As can be seen from the simulation results, 29.67% of the heavy oil has been converted only in the feed mixing zone compared to 64.54% converted by the whole riser reactor. In other words, nearly half of the heavy-oil conversion takes place in the region between the heavy-oil injection nozzles and the outlet of the feed mixing section. This region is only one-fifth of the overall riser height. For propylene, ethylene, and liquid product conversion at the outlet of the feed mixing region, the yields reach 8.84%, 4.39%, and 92.42%, respectively, which are very close to the yields obtained at the riser outlet. These results further substantiate the importance of the feed mixing section of the riser reactor. Consequently, improving the gas−solid contact efficiency in the feed mixing section is of crucial importance in obtaining better product profiles.

Figure 5 depicts the catalyst activity profile contour. The catalyst activity was calculated based on the catalyst deactivation function. In the prelifting part, few reactions take place, so the catalyst has a high reaction activity in this region. As the reactions mainly take place in the vicinity of both the heavy-oil and light-gasoline feed nozzles, the catalyst activity drops sharply in these regions. Therefore, it is of vital importance to improve the feed-oil atomization and vaporization efficiency to convert as much feed oil as possible. In addition, similarly to the solid flow field, the catalyst activity shows an obvious bias flow profile because of the downward oblique nozzle. On the oblique downward nozzle side, the catalyst activity is higher than that on the offside. Therefore, it is necessary to add another downward oblique

Table 8. Comparison of the Outlet Compositions of the Feed Mixing Section and the Whole Riser (wt %)

		simulation results	
term	experimental data	whole riser	feed injection zone
recycle oil	14.57	12.65	28.90
diesel oil	2.54	4.37	1.71
gasoline	49.47	43.49	45.05
LPG	25.54	27.09	16.80
dry gas + coke + loss	7.88	12.32	7.58
total	100	100	100
conversion (to recycle oil)[a]	64.54	69.21	29.67
propylene	–	14.01	8.84
ethylene	–	6.58	4.39
yield of liquid product	92.12	87.68	92.42

[a] Conversion (to recycle oil) = 1 − {[recycle oil (product)]/[recycle oil (feed)]}, where recycle oil (feed) = 41.07%.

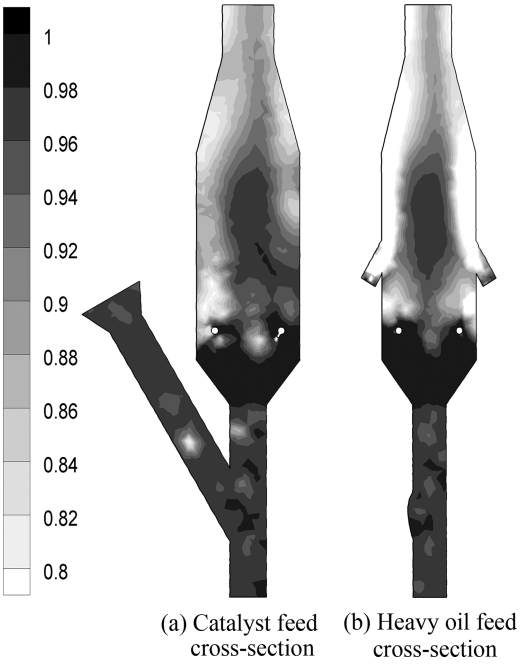

Figure 5. Catalyst activity in the TMP feed injection zone.

nozzle on the offside to form a bilaterally symmetrical flow or to let some of the nozzles be oblique downward, which might weaken the bias flow and improve the solid density and activity in the upper region.

Figure 6 shows the main generating region of the cracking reaction products. The darker the color, the higher the generation rate. For the different products, the generation rates and production regions are distinct. It can be easily observed that diesel oil is mainly produced near the heavy-oil nozzles and in the near-wall region of the feed mixing zone, gasoline is produced in the vicinity of the lower layer of oil nozzles and the central region

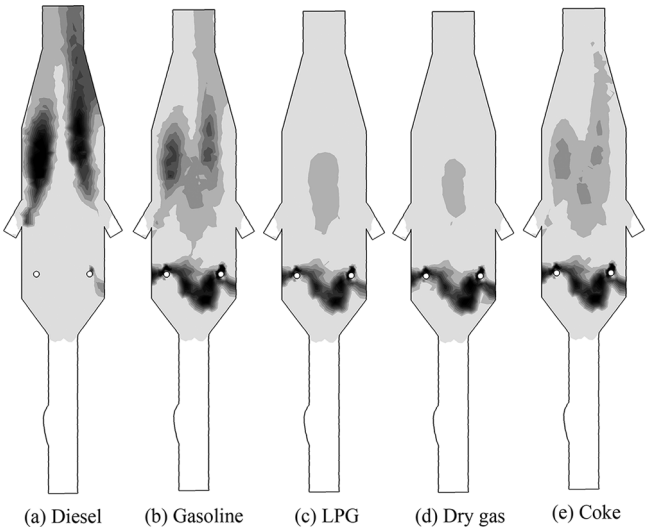

Figure 6. Main generating region of the lumps.

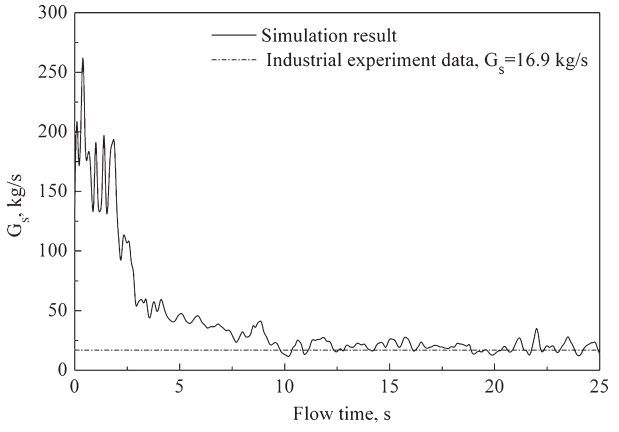

Figure 7. Distribution of solid volume fraction on the axis in the laboratory-scale riser reactor.

above there, and light products (LPG and dry gas) are mainly generated in the vicinity of the light-oil nozzles. Coke, which is a final product, is generated in both regions mentioned above. In addition, the reaction rate in the upper zone of the riser is much lower than that in the feeding zone, which emphasizes the importance of ensuring better contact between the oil and the catalyst in this region.

The above simulation results explain the flow and cracking reaction pattern in terms of the hydrodynamics and reaction kinetics. This information can play a valuable role in optimizing the geometry of the industrial riser reactor. It is known that investigating hydrodynamic conditions in real industrial reactors is difficult, although the overall mass flux of catalyst particles can be measured and used as a factor to evaluate the precision of the CFD simulations. The mass flux of catalyst particles in the industrial reactor is compared with the CFD results in Figure 7. Good agreement between the industrial reactor measurements and numerical results is observed.

The predominance of the novel multiregime riser reactor can also be visually confirmed by the product distribution of the industrial results (see Table 9). The propylene yields approaches

Table 9. Benchmark Results of the 120 kton/year Industrial Plant (wt %)

term	first stage	second stage	total	design
feedstock	fresh feed, 81.68	recycle oil, 41.07		
	mixed C_4, 18.32	light gasoline, 58.93	100	100
	total, 100.00	total, 100.00		
recycle oil	13.75	14.57	2.67	1.3
diesel oil	9.90	2.54	17.42	19.00
gasoline	31.33	49.47	28.6	27.20
LPG	36.23	25.54	36.77	37.5
off gas + coke + loss	8.78	7.88	14.54	15.00
total	100	100	100	100
propylene	–	–	19.64	18−20
conversion	83.16 (to fresh feed)	64.54 (to recycle oil)	83.26	
light-oil yield	41.23	52.01	47.06	
aimed product yield	77.46	66.58	81.59	
total liquid yield	91.22	92.12	84.96	85

20%, and gasoline and diesel quality still remains at an acceptable level. Also, good agreement with the design conditions can be concluded from the benchmark results. These results further indicate that, with a suitable reaction temperature and optimized feed pattern (such as suitable injection direction of the light-oil nozzles), the TMP process can obtain higher LPG yields, in particular, for propylene.

6. CONCLUSIONS

Numerical simulations in which the fluid flow was coupled to cracking reactions were conducted to verify the performance of a novel multiregime gas−solid fluidized reactor for heavy-oil catalytic pyrolysis. The numerical findings are in good agreement with test run results of a real industrial unit. This novel process demonstrates its superiority over other catalytic cracking/pyrolysis process. The numerical work provided more detailed insights into the cracking process: (i) The catalyst distribution of the changing-diameter riser is better than that of the traditional riser; various fluidized regimes could be integrated in a single reactor. (ii) The multiregime gas−solid reactor provides better control of fast reaction systems, especially for heavy-oil catalytic cracking. (iii) The cracking reactions mainly take place in the feed mixing section; hence, optimizing the oil and catalyst contact in this region is of vital importance.

AUTHOR INFORMATION

Corresponding Author

*Fax: +86-532-8698-4711 (H.Z.), +971-260-75200 (A.S.B.). E-mail: zhaohui@upc.edu.cn (H.Z.), aberrouk@pi.ac.ae (A.S.B.).

ACKNOWLEDGMENT

Financial support for this project provided by National Basic Research Program of China (2012CB215006), TAKREER (Abu Dhabi Oil Refining Company) operating company of the Abu Dhabi National Oil Company (ADNOC), and the Fundamental

Research Funds for the Central Universities of China is gratefully acknowledged.

NOMENCLATURE

A = cross-sectional area, m^2
C_D = drag coefficient
d_s = particle diameter, m
e = coefficient of restitution
e_w = restitution coefficient at the wall
E_a = apparent activation energy, $kJ \cdot mol^{-1}$
g = gravity, $m \cdot s^{-2}$
G_s = solid circulating rate, $kg \cdot m^{-2} \cdot s^{-1}$
k_0 = frequency factors, s^{-1}
P = pressure, Pa
Q_{rj} = reaction heat of component j, $J \cdot m^{-3} \cdot s^{-1}$
Q_{sg} = interphase heat transfer, $J \cdot m^{-3} \cdot s^{-1}$
Re = Reynolds number
V = velocity, $m \cdot s^{-1}$
W_j = reaction rate of component j, $kg \cdot m^{-3} \cdot s^{-1}$
Y_j = mass fraction of component j

Greek Letters

β = drag coefficient
ΔH_r = reaction heat, $kJ \cdot kg^{-1}$
ε = volume fraction
Θ_s = granular temperature, $m^2 \cdot s^{-2}$
λ = bulk viscosity, $Pa \cdot s$
μ = shear viscosity, $Pa \cdot s$
μ_{eff} = effective viscosity, $Pa \cdot s$
ρ = density, $kg \cdot m^{-3}$
τ = stress
ω = drag force modify coefficient

Subscripts

g = gas phase
s = solid phase

REFERENCES

(1) Zou, L. Q.; Gu, X. W.; Zhang, H. Z. Application of ARGG in Fluid Catalytic Cracking. *Pet. Technol.* **1998**, *27*, 756.

(2) Xie, C. G. Commercial Application of Deep Catalytic Cracking Catalysts for Production of Light Olefins. *Pet. Technol.* **1997**, *26*, 825.

(3) Yang, Y. G.; Luo, Y. Commercial application of DCC-II and its flexibility on production. *Pet. Process. Petrochem.* **2000**, *31*, 1.

(4) Han, W. D.; Huang, R. K.; Gong, J. H. Commercial application of new FCC process MIP-CGP. *Pet. Refinery Eng.* **2006**, *36*, 1.

(5) Wang, L. Y.; Wang, G. L.; Wei, J. L. New FCC process minimizes gasoline olefin, increases propylene. *Oil Gas J.* **2003**, *101*, 52.

(6) Li, C. Y.; Yang, C. H.; Shan, H. H. Maximizing propylene yield by two-stage riser catalytic cracking of heavy oil. *Ind. Eng. Chem. Res.* **2007**, *46* (14), 4914–4920.

(7) Li, Z. Q.; Wu, C. N.; Wei, F.; Jin, Y. Experimental study of high-density gas−solids flow in a new coupled circulating fluidized bed. *Powder Technol.* **2004**, *139* (3), 214–220.

(8) Qi, X.; Zhu, J.; Huang, W. Hydrodynamic similarity in circulating fluidized bed risers. *Chem. Eng. Sci.* **2008**, *63* (23), 5613–5625.

(9) Qi, X.-B.; Zhang, H.; Zhu, J. Solids concentration in the fully developed region of circulating fluidized bed downers. *Powder Technol.* **2008**, *183* (3), 417–425.

(10) Han, I.-S.; Chung, C.-B.; Riggs, J. B. Modeling of a fluidized catalytic cracking process. *Comput. Chem. Eng.* **2000**, *24* (2−7), 1681–1687.

(11) Das, A. K.; Baudrez, E.; Marin, G. B.; Heynderickx, G. J. Three-Dimensional Simulation of a Fluid Catalytic Cracking Riser Reactor. *Ind. Eng. Chem. Res.* **2003**, *42* (12), 2602–2617.

(12) Lan, X. Y.; Xu, C. M.; Wang, G.; Wu, L.; Gao, J. S. CFD modeling of gas−solid flow and cracking reaction in two-stage riser FCC reactors. *Chem. Eng. Sci.* **2009**, *64*, 3847–3858.

(13) Ancheyta-Juárez, J.; López-Isunza, F.; Aguilar-Rodríguez, E. 5-Lump kinetic model for gas oil catalytic cracking. *Appl. Catal. A: Gen.* **1999**, *177*, 227–235.

(14) Bollas, G. M.; Lappas, A. A.; Iatridis, D. K.; Vasalos, I. A. Five-lump kinetic model with selective catalyst deactivation for the prediction of the product selectivity in the fluid catalytic cracking process. *Catal. Today* **2007**, *127* (1−4), 31–43.

(15) Jacob, S. M.; Gross, B.; Voltz, S. E.; Weekman, V. W. A lumping and reaction scheme for catalytic cracking. *AlChE J.* **1976**, *22* (4), 701–713.

(16) Lee, L. S.; Chen, Y. W.; Huang, T. N.; Pan, W. Y. Four lump kinetic model for FCC process. *Can. J. Chem. Eng.* **1989**, *67*, 615–619.

(17) Xu, Y. H. Establishment of kinetic model for dcc and its application. *Pet. Refinery Chem. Eng.* **2001**, *32* (11), 44–47.

(18) Meng, X. H.; Gao, J. S.; Xu, C. M.; Li, L. Studies on the Kinetic Model of Daqing Atmospheric Residue Catalytic Proylsis. *Chem. React. Eng. Technol.* **2003**, *19* (4), 365–370.

(19) Wang, G. L.; Wang, L. Y.; Cui, Z.; Liu, J.; Liu, X. F. Study on Lumped Kinetic Reaction Network of Heavy Oil Contact Cracking Process. *Petrochem. Technol.* **2004**, *33* (2), 93–99.

(20) Li, L.; Gao, J. S.; Xu, C. M.; Meng, X. H. Study on lumping kinetic model of heavy oil catalytic pyrolysis. *Mod. Chem. Ind.* **2006**, *26* (suppl 2), 338–346.

(21) Guo, J. H.; Zhao, H.; Liang, Z. T.; Wang, H. G.; Yang, C. H. Study on the kinetic model of heavy oil catalytic pyrolysis. In *Proceeding of Qilu Graduate Academic Forum − Chemical Engineering and Technology Session Dongying, China, 2007*; China University of Petroleum Press: Dongying, China, 2007; pp 52−60.

(22) Guo, J. H. Primary Study of the Lumped Kinetic Model for Heavy Oil Cracking into Propylene by Two-Stage-Riser Technology. M.S. Thesis, China University of Petroleum, Dongying, China, 2007.

(23) Cai, F. P.; Fan, Y. P.; Shi, M. X. Structure and flow field of a novel feedstock mixing zone in the nozzle of FCC riser. *Pet. Process. Petrochem.* **2004**, *35* (12), 37–41.

(24) Fan, Y. P.; E, C. L.; Shi, M. X.; Xu, C. M.; Gao, J. S.; Lu, C. X. Diffusion of Feed Spray in Fluid Catalytic Cracker Riser. *AIChE J.* **2010**, *56* (4), 858–868.

(25) Yang, C. H.; Shan, H. H.; Zhang, J. F. Two-stage riser FCC technologies. *Pet. Refinery Eng.* **2005**, *35* (3), 28–33.

(26) Li, X. H. Fundamental Studies on the Technology of Fluid Catalytic Cracking with Two-Stage Risers for Maximizing Propylene. Ph.D. Thesis, China University of Petroleum, Dongying, China, 2007.

(27) Liu, Q. H.; Niu, G. L.; Yang, C. H. Study on particle flow characteristics in new structure FCC riser. *Pet. Refinery Eng.* **2007**, *37* (10), 32–36.

(28) Buchanan, J. S. Analysis of heating and vaporization of feed droplets in fluidized catalytic cracking risers. *Ind. Eng. Res. Dev.* **1994**, *33*, 3104–3111.

(29) Jin, W. L. Cracking Heat of MGG Technology. *Catal. Cracking* **1995**, *3*, 1–9.

(30) Gidaspow, D. *Multiphase Flow and Fluidization: Continuum and Kinetic Theory Descriptions*; Academic Press: New York, 1994.

(31) Wen, C. Y.; Yu, Y. H. A generalized method for predicting the minimum fluidization velocity. *AICHE J.* **1966**, *12*, 610.

(32) Di Felice, R. The voidage function for fluid−particle interaction systems. *Int. J. Multiphase Flow* **1994**, *20*, 153.

(33) Ergun, S. Fluid flow through packed columns. *Chem. Eng. Prog.* **1952**, *48*, 89.

(34) Gidaspow, D.; Jung, J.; Singh, R. Hydrodynamics of fluidization using kinetic theory: an emerging paradigm. *Powder Technol.* **2004**, *148*, 123–141.

(35) Syamlal, M.; O'Brien, T. J. Computer Simulation of Bubbles in a Fluidized Bed. *AIChE Symp. Ser.* **1989**, *85*, 22–31.

(36) Yang, N.; Wang, W.; Ge, W.; Li, J. H. CFD simulation of concurrent-up gas−solid flow in circulating fluidized beds with structure-dependent drag coefficient. *Chem. Eng. J.* **2003**, *96* (1−3), 71–80.

(37) Li, J. H.; Wen, L. X.; Ge, W.; Cui, H. P.; Ren, J. Q. Dissipative structure in concurrent-up gas−solid flow. *Chem. Eng. Sci.* **1998**, *53* (19), 3367–3379.

(38) Johnson, P. C.; Jackson, R. Frictional−collisional constitutive relations for granular materials, with application to plane shearing. *J. Fluid Mech.* **1987**, *176*, 67–93.